Radiat Environ Biophys (2012) 51:43–52
DOI 10.1007/s00411-011-0388-3

ORIGINAL PAPER

Damage clusters after gamma irradiation of a nanoparticulate plasmid DNA peptide condensate

Trinh T. Do · Vicky J. Tang · Katie Konigsfeld · Joe A. Aguilera · Chris C. Perry · Jamie R. Milligan

Received: 2 March 2011 / Accepted: 18 September 2011 / Published online: 2 October 2011

Abstract We have gamma-irradiated plasmid DNA in aqueous solution in the presence of submillimolar concentrations of the ligand tetra-arginine. Depending upon the ionic strength, under these conditions, the plasmid can adopt a highly compacted and aggregated form which attenuates by some two orders of magnitude the yield of damage produced by the indirect effect. The yields of DNA single- and double-strand breaks (SSB and DSB) which result are closely comparable with those produced in living cells. The radical lifetimes, diffusion distances, and track structure are expected to be similarly well reproduced. After irradiation, the aggregation was reversed by adjusting the ionic conditions. The approximate spatial distribution of the resulting DNA damage was then assayed by comparing the increases in the SSB and DSB yields produced by a subsequent incubation with limiting concentrations of the eukaryotic base excision repair enzymes formamidopyrimidine-DNA *N*-glycosylase (the FPG protein) and endonuclease III. Smaller increases in DSB yields were observed in the plasmid target that was irradiated in the condensed form. By modeling the spatial distribution of DNA damage, this result can be interpreted in terms of a greater extent of damage clustering.

T. T. Do · V. J. Tang · K. Konigsfeld · J. A. Aguilera · J. R. Milligan (✉)
Department of Radiology, University of California at San Diego, 9500 Gilman Drive, La Jolla, CA 92093-0610, USA
e-mail: jmilligan@ucsd.edu

C. C. Perry
Department of Biochemistry, Mortensen Hall, Loma Linda University, 11085 Campus Street, Loma Linda, CA 92350, USA

Introduction

The DNA damage produced by ionizing radiation (such as X-rays and gamma rays) appears to be uniquely effective at producing biological effects such as cell lethality (Ward 1994). The yields of well-characterized DNA damage events such as strand breaks, adducts, or dimerized bases produced by other lethal agents such as oxidizing agents, alkylating agents, or non-ionizing radiation (UV photons) required to produce comparable numbers of lethal events are three to four orders of magnitude greater than is the case even for sparsely ionizing or low LET radiation. This effect is widely attributed to the non-uniform track structure of energy deposition produced by ionizing radiations (Goodhead 1994; Nikjoo et al. 2002) and the limited opportunity for diffusion or migration of the reactive intermediates (such as the hydroxyl radical) that are produced in a biological target.

In dilute aqueous solutions containing a DNA target, the efficiency of the direct effect is roughly proportional to the fraction of the mass it contributes to the target. For typical cell-free experimental DNA concentrations in the approximate range of 1 μg ml^{-1}–1 mg ml^{-1}, the value is necessarily less than one part in a thousand. Consequently, the resulting DNA damage is dominated by the indirect effect. As a result, our understanding of the indirect effect is far better developed than that of the direct effect (von Sonntag 2006; Pogozelski and Tullius 1998). Experimental systems that seek to characterize direct-type DNA damage must attenuate this otherwise overwhelmingly large contribution of the indirect effect. Well-established experimental methods to achieve this involve dehydration (to prevent the formation of water-derived radicals), freezing (to prevent their diffusion), adding large concentrations of scavengers (to chemically modify them to less reactive species), or the

use of single-electron oxidizing agents (to simulate ionization of guanine, the most easily oxidized site in DNA). While widely practiced in the physical sciences, none of the first three of these techniques represents a close approximation to physiological conditions. They also have a limited ability to reproduce the reactivity of the resulting reactive intermediates with water and oxygen, two reagents whose chemical reactivity with cations, anions, and radicals is central to radiobiology (von Sonntag 2006). The fourth tends to model poorly the issue of radical lifetime and diffusion distance and therefore cannot address the unique aspect of DNA damage by ionizing radiation: the track structure. It would therefore appear to be desirable to develop additional model systems with which to study the direct effect, and the use of condensed DNA appears to offer one such possibility.

There is strong evidence from a variety of experimental systems that the issue of DNA compaction is strongly related to the yields of DNA damage (Spotheim-Maurizot et al. 1995; Newton et al. 1996; Chiu and Oleinick 1998; Warters et al. 1999). We employ here a model system involving plasmid DNA condensed with a relatively inert cationic oligopeptide. It provides a convenient means to attenuate extensively the otherwise overwhelmingly large contribution made in aqueous solutions by the indirect effect. As a result, it is possible to reproduce closely the low SSB and DSB yields observed in living cells (Newton et al. 1996, 1997) with a dilute aqueous solution containing submillimolar concentrations of a peptide ligand. Such a system bears a much closer resemblance to physiological conditions than other commonly used models for the direct and quasi-direct effects (i.e., dehydration and freezing). Using a cationic ligand, the low yields result from a highly scavenged environment in the neighborhood of the DNA target. The limited radical diffusion distances under these circumstances argue that the spatial distribution of the resulting DNA damage is strongly representative of the track structure of energy deposition by ionizing radiation in mammalian cells. By later increasing the ionic strength to dissociate the electrostatically bound ligand (Bloomfield 1996), the damage in the resulting regular uncondensed DNA may be assessed by using existing analytical methods. Such an experimental system reproduces fairly well the packing density of the nucleosomal structure of mammalian DNA (Daban 2003). The use of a peptide ligand that can incorporate additional amino acids (Milligan et al. 2003) provides a better approximation to the chemical reactivity expected from DNA-binding proteins than the other classes of cationic ligands mentioned above. We report here the application to a gamma-irradiated-condensed plasmid DNA target of a previously described assay for DNA damage clustering (Milligan et al. 2000). This assay involves comparison with one another the increases in the SSB and DSB yields after incubation of the irradiated DNA with limiting concentrations of base excision repair endonucleases.

Materials and methods

Biochemicals

Plasmid pHAZE (length 1.03×10^4 base pairs, Lutze and Winegar 1990) was grown to a milligram scale in an *E. coli* host. We have previously described its extraction and purification to the standards required by radiation chemistry (Milligan et al. 1993). The base excision repair endonucleases formamidopyrimidine-DNA *N*-glycosylase (FPG) and endonuclease III (endo III) were obtained from Trevigen (Gaitherburg, MD). Recombinant bovine enteric DNAse I was obtained from Roche (Indianapolis, IN). Tetra-arginine (R_4^{4+}) was obtained from Biomatik (Wilmington, DE).

Composition of plasmid–ligand mixtures

Aqueous solutions of plasmid pHAZE (100 μg ml^{-1}, 3.1×10^{-4} mol l^{-1} nucleotide residues, 1.5×10^{-8} mol l^{-1} plasmid macromolecules) were prepared in the presence of a buffer system (5×10^{-3} mol l^{-1} sodium phosphate, pH 7.0), and in some cases, sodium perchlorate (5×10^{-2} mol l^{-1}). Glycerol (zero, or 5×10^{-6}–2 mol l^{-1}) and tetra-arginine (zero, or 1×10^{-6}–6×10^{-4} mol l^{-1}) were also present. For those solutions containing tetra-arginine, it was added last, and the resulting mixture was allowed to stand at room temperature for 1 h. The necessity for such precautions has been reported in the literature (Vilfan et al. 2006).

Sedimentation

The supernatant solution was recovered after centrifugation at 15,000×*g* for 20 min.

Static light scattering

The static intensity of light scattered at a nominal angle of 90° was quantified using a model F-7000 fluorescence spectrophotometer (Hitachi, Pleasanton, CA) with excitation and emission monochromators set to a wavelength of 400 nm (both bandwidths 5 nm). The sample volume was 200 μl.

Dynamic light scattering

The size distribution of solutions or suspensions was quantified by dynamic light scattering using a model 370 instrument (Nicomp, Santa Barbara, CA). The coherent

illumination source was an He–Ne laser (632 nm, 60 mW). Time-resolved data were collected at a nominal scattering angle of 90°. It was fitted with a proprietary autocorrelation function. The distribution of the diffusion coefficient was derived from this function by the inverse Laplace transform method. The apparent spherical hydrodynamic radius was then calculated from the diffusion coefficient using the Stokes–Einstein equation. The sample volume was 1 ml.

UV spectroscopy

UV–visible absorption spectra were measured using a model DU-800 spectrophotometer (Beckman Coulter, Fullerton, CA). The sample volume was 150 µl.

Fluorescence spectroscopy

The fluorescence intensity was examined in the additional presence of 5×10^{-7} mol l^{-1} ethidium bromide. Emission spectra were recorded using a model F-7000 fluorescence spectrophotometer (Hitachi, Pleasanton, CA). The excitation wavelength was 480 nm (bandwidth 5 nm). The emission intensity was recorded from 500 to 700 nm (bandwidth 5 nm). The sample volume was 200 µl.

Nuclease digestion

The sensitivity of the plasmid to digestion by DNAse I was estimated from a 60-min incubation at 37°C in the additional presence of 1×10^{-4} mol l^{-1} magnesium acetate and 0.2–5 $\times 10^{-4}$ units μl^{-1} DNAse I. The sample volume was 16 µl. The reaction was halted by the addition of 10^{-1} mol l^{-1} EDTA (4 µl). The plasmid was then assayed for strand breaks by agarose gel electrophoresis. The efficiency of the formation of DNA single-strand breaks (SSB) was estimated from the slope of a plot of the number of SSB events per plasmid (assuming a Poisson distribution this is equal to the natural logarithm of the reciprocal of the fraction of the plasmid remaining in the supercoiled form, see below) against the enzyme concentration. The efficiency was calculated with units of SSB events per plasmid per unit activity of DNAse I per ml.

Gamma irradiation

Aliquots (5 µl, no enzyme incubation; or 50 µl, with a later enzyme incubation) were gamma-irradiated (662 keV photon) using an isotopic cesium-137 source in a Gamma-Cell-1000 instrument (J. L. Shepherd, San Fernando, CA). The dose rate of 4.8×10^{-2} Gy s^{-1} was calibrated using the Fricke system (Spinks and Woods 1990) and commercial luminescence-based dosimeters (Landauer, Glenwood, IL). Radiation doses were in the range of 0.2–300 Gy.

Post-irradiation incubation

After irradiation, the aliquots were treated with 2 mol l^{-1} aqueous sodium perchlorate to a final concentration of 0.1 mol l^{-1}, in order to reverse any condensation. Those samples not requiring any enzyme incubation were diluted to a final volume of 20 ml with a solution containing sodium phosphate (5×10^{-3} mol l^{-1}, pH 7.0) and sodium perchlorate (0.1 mol l^{-1}). Those samples receiving a subsequent incubation were separated into smaller aliquots (5 µl) and treated with a solution (15 µl) containing both FPG and endo III at various dilutions, sodium phosphate (5×10^{-3} mol l^{-1}, pH 7.0) and sodium perchlorate (0.1 mol l^{-1}). The final concentrations of FPG and endo III were in the range of 2–20 unit ml^{-1} and 20–200 units ml^{-1}, respectively. All samples were then incubated at 37°C for 30 min.

Agarose gel electrophoresis

After DNAse I incubation, or gamma irradiation and subsequent incubation with (if applicable) the enzymes FPG and endo III, the sample aliquots (20 µl) were treated with a loading buffer (5 µl) containing sucrose (40%) and bromophenol blue (1 mg ml^{-1}). The resulting solutions were loaded into a 0.6 × 10 × 20 cm 0.8% agarose gel and subjected to electrophoresis for 13 h using the TBE buffer system (9×10^{-2} mol l^{-1} Tris, 9×10^{-2} mol l^{-1} boric acid, 1×10^{-3} mol l^{-1} EDTA) at an electric field of 2.2 V cm^{-1} and a current of 25 mA.

Strand break yields

After electrophoresis, the fraction of the plasmid in the supercoiled (break free), open circle (containing at least one SSB), and linear (containing one double-strand break (DSB)) forms was quantified by digital video imaging using a Gel Doc XR instrument (Bio-Rad, Hercules, CA) of their ethidium fluorescence (Milligan et al. 1993). The D_0 gamma radiation dose is defined as the dose required to decrease, by a factor of e, the fraction of SSB-free plasmid. Assuming a Poisson distribution, this is equivalent to introducing a mean of one SSB per plasmid. The value of D_0 is equal to the reciprocal of the slope m of a straight line fitted to a semilogarithmic yield dose plot. At the D_0 dose, the concentration of the SSB product is equal to the concentration of the plasmid during irradiation (1.5×10^{-8} mol l^{-1}, see above). Therefore, the radiation chemical yield or G-value for SSB formation (units of mol J^{-1}) may be calculated by dividing this concentration by the value of D_0. Similarly, the G-value for DSB formation was calculated from the initial slope of a yield dose plot of the formation of the linearized form of the plasmid. For example yield dose plots are described below.

Results

The behavior of the plasmid pHAZE in the presence of the ligand tetra-arginine (R_4^{4+}) was characterized by using UV spectroscopy, ethidium fluorescence, and the enzyme DNAse I (Fig. 1). After a brief centrifugation, the concentration of the plasmid in the supernatant solution was quantified using its UV absorption at 260 nm. At R_4^{4+} concentrations up to 5×10^{-5} mol l^{-1}, all of the plasmid remained in solution. At R_4^{4+} concentrations of 7×10^{-5} mol l^{-1} and above, the centrifugation step was able to pellet the vast majority of the plasmid, and it was no longer detectable in the supernatant.

The plasmid was also characterized both before and after centrifugation by means of the fluorescence intensity of the dye ethidium, which was present at a concentration 600-fold lower than that of the plasmid (in terms of nucleotide residues). Before centrifugation, at R_4^{4+} concentrations from zero to 5×10^{-5} mol l^{-1}, the fluorescence emission spectrum characteristic of bound ethidium with a maximum at 593 nm was observed, having a constant intensity. At R_4^{4+} concentrations of 7×10^{-5} mol l^{-1} and above, three effects were apparent. The location of the emission maximum decreased by 5 nm, the emission band became less broad, and its intensity decreased by ca. 40%. Only the largest of these effects, the decrease in intensity, is depicted in Fig. 1. After centrifugation, the intensity of the fluorescence detected in the supernatant showed very little change at ligand concentrations up to 5×10^{-5} mol l^{-1}. At the higher ligand concentrations, the intensity decreased to a very low level.

The reactivity of the plasmid with DNAse I decreased slightly by ca. fivefold as the ligand concentration increased from 5×10^{-6} to 5×10^{-5} mol l^{-1}. It decreased by a further ca. 100-fold at a ligand concentration of 8×10^{-5} mol l^{-1}.

The physical effect of R_4^{4+} on the plasmid was also assessed by using static and dynamic light scattering (Fig. 2). Static light scattering (SLS) was examined at 400 nm. This wavelength is short enough to provide adequate sensitivity, but long enough that the bases in the plasmid exhibit a negligible absorption. SLS was examined both before and after a brief centrifugation. Before centrifugation, the intensity of light scattering increases by ca. 100-fold as the R_4^{4+} concentration is increased by ca. twofold from 3×10^{-5} to 7×10^{-5} mol l^{-1}. Concentrations below the lower limit of 3×10^{-5} mol l^{-1} and above the upper limit of 7×10^{-5} mol l^{-1} have essentially no additional effect on the SLS intensity. This large light scattering signal was no longer observable after centrifugation, and instead, the intensity was slightly lower than in the absence of any added R_4^{4+}.

We also used time-resolved or dynamic light scattering (DLS) of a 630-nm coherent light source, for the purpose of estimating the size range of the particles responsible for the SLS signal. This assay reported an essentially monodisperse size distribution with a standard deviation of the same order as the symbol size in Fig. 2. The mean particle size increased by ca. 13-fold from ca. 150 to ca. 2,000 nm as the R_4^{4+} concentration was increased from 2×10^{-5} to 7×10^{-5} mol l^{-1}.

In addition, the large SLS and sedimentation effects evident at a ligand concentration of 1.4×10^{-4} mol l^{-1} (in ca.

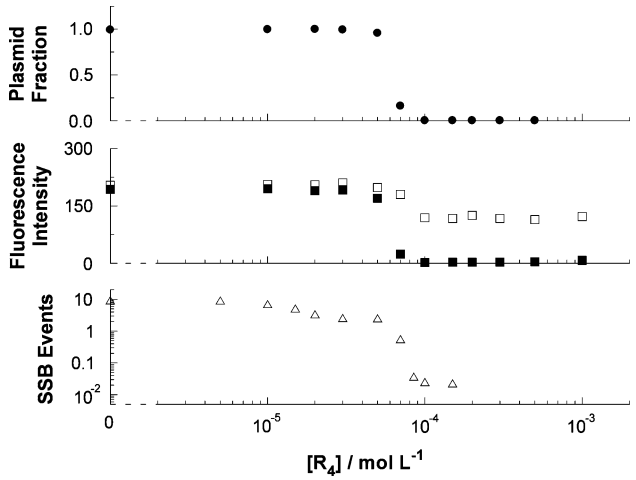

Fig. 1 Effect of the concentration of the ligand R_4^{4+} on the properties of plasmid pHAZE. These are the following: the fraction of the plasmid remaining in the supernatant after sedimentation (*upper panel*, *circular symbols*); the ethidium fluorescence intensity before (*open symbols*) and after (*closed symbols*) sedimentation (*middle panel*, *square symbols*); and the number of SSB events produced in the plasmid by DNAse I (*lower panel*, *triangular symbols*)

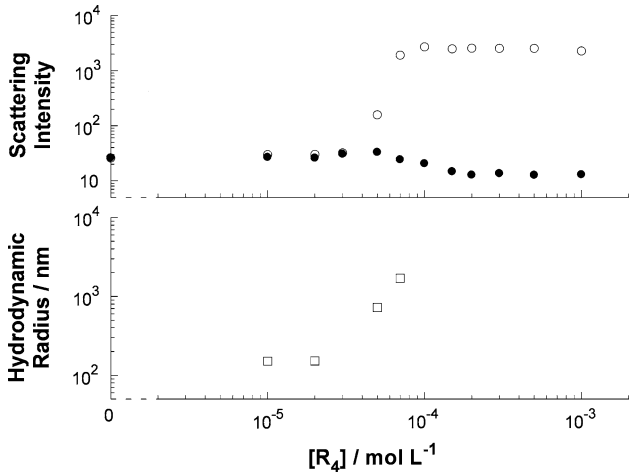

Fig. 2 Effect of the concentration of the ligand R_4^{4+} on light scattering by pHAZE. Static light scattering was determined before (*open symbols*) and after (*closed symbols*) sedimentation (*upper panel*, *circular symbols*); the hydrodynamic radius was determined before sedimentation by dynamic light scattering (*lower panel*, *square symbols*)

twofold excess of that required to produce these effects) were not observed in the additional presence of 5×10^{-2} mol l^{-1} sodium perchlorate (not shown). Increasing the ionic strength in this manner has the effect of inhibiting the binding of the ligand to the plasmid. We have previously reported on very similar behavior with the ligands tetra-lysine (Newton et al. 2004) and penta-arginine (Tsoi et al. 2010).

We wished to examine the effect of the presence of the ligand R_4^{4+} on the sensitivity of the plasmid to ionizing radiation. The results of a representative experiment are reproduced in Fig. 3. Here, plasmid pHAZE was gamma-irradiated in the presence of 1.4×10^{-4} mol l^{-1} R_4^{4+} and 5×10^{-2} mol l^{-1} sodium perchlorate. After irradiation, aliquots were incubated in the presence of the enzymes FPG and endo III. As the gamma dose was increased from zero to 3 Gy, the fraction of the plasmid remaining in the supercoiled conformation decreased from 0.9 to 0.1. Incubation with the two base excision repair enzymes accelerated with dose-related decrease. Gel electrophoresis revealed that the supercoiled form of the plasmid was converted predominantly into the relaxed or open circle form, so the loss of the supercoiled form corresponds to the introduction into the plasmid of DNA single-strand breaks (SSB). From the slopes of the yield dose plots in Fig. 3, it is possible to calculate the radiation chemical yields (G-values) in which these SSB events are produced by the gamma radiation and therefore also the factor by which this yield is increased by any subsequent enzyme incubation. For the data plotted in Fig. 1, these G(SSB) values are 1.04×10^{-2} and 1.52×10^{-2} μmol J^{-1}, leading to a 1.52/1.04 = 1.46-fold increase.

With higher radiation doses, it was also possible to observe the formation of DNA double-strand breaks in pHAZE. An example is reproduced in Fig. 4, where both the irradiation and incubation conditions were identical to those for Fig. 3. The fraction of the linearized plasmid increased with radiation dose, and this increase was larger after the enzyme incubation. From the initial slopes of the lines fitted to the data, it is possible to derive quantitative estimates for the yields of double-strand breaks (G(DSB) values). The values obtained from Fig. 4 without and with enzyme incubation are, respectively, 7.09×10^{-5} and 1.67×10^{-4} μmol J^{-1}. This leads to an estimate of the effect of the enzyme incubation as an increase by a factor of 1.67/0.709 = 2.36 in the DSB yield.

As mentioned in the Introduction, we wished to assess the effects of the presence during irradiation of the ligand R_4^{4+} on the SSB and DSB yields. Examples of SSB and DSB yields (with irradiation in the absence of any added sodium perchlorate and with subsequent incubation in the absence of any added enzymes) are shown in Fig. 5. For comparative purposes, the effect of the commonly used hydroxyl radical scavenger glycerol was also examined. With glycerol, both the SSB and DSB yields decreased

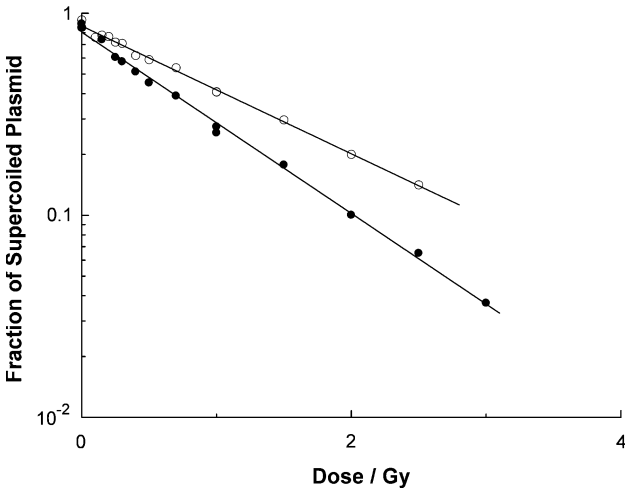

Fig. 3 Loss of supercoiled plasmid resulting from gamma irradiation with and without subsequent enzyme incubation. A solution containing plasmid pHAZE (100 μg ml^{-1}), phosphate (5×10^{-3} mol l^{-1}), sodium perchlorate (5×10^{-2} mol l^{-1}), and tetra-arginine (R_4^{4+}, 1.4×10^{-4} mol l^{-1}) was irradiated under aerobic conditions with cesium-137 gamma rays to the doses indicated on the horizontal X-axis. The fraction of intact supercoiled plasmid remaining after each dose was determined by agarose gel electrophoresis. After irradiation but before electrophoresis, the plasmid was incubated for 30 min at 37°C under one of two different conditions: (1) in the absence of any added enzyme (*open circle*) or (2) with both 20 unit ml^{-1} FPG and 100 unit ml^{-1} endo III (*closed circle*). Both data sets were fitted with least mean square straight lines of the form $y = ce^{-mx}$. From the slopes m of these lines, the D_0 doses radiation chemical yields for SSB formation under these conditions were found to be: (1, neither enzyme) 1.43 Gy, 1.04×10^{-2} μmol J^{-1}; and (2, both enzymes) 0.981 Gy, 1.52×10^{-2} μmol J^{-1}

gradually by ca. 100-fold as the glycerol concentration was increased from 1×10^{-4} to 2 mol l^{-1}.

In contrast, the effect of the ligand R_4^{4+} was very different from that of glycerol. It was also able to produce the ca. 100-fold decrease in both SSB and DSB yields, but this large attenuation was observed over a very narrow range of concentration in the region of 6×10^{-5}–8×10^{-5} mol l^{-1} (an increase of less than 1.5-fold), while glycerol required an increase in concentration of four orders of magnitude. This sharp decrease in the strand break yields took place under the same conditions that also produced the large changes in physical properties such as sedimentation, ethidium fluorescence, and light scattering (Figs. 1, 2).

Since we wished to employ a post-irradiation nuclease incubation as a means to assay the DNA damage produced by gamma irradiation in the condensed form, it was necessary to use a means to reverse the aggregation in order to permit access of the base excision repair endonucleases FPG and endo III. As mentioned above, the non-specific electrostatic binding of the cationic ligand to the polyanionic plasmid is well known to be highly sensitive to the ionic strength (Bloomfield 1996; Padmanabhan et al. 1997). An example of this effect is shown in Fig. 6, where

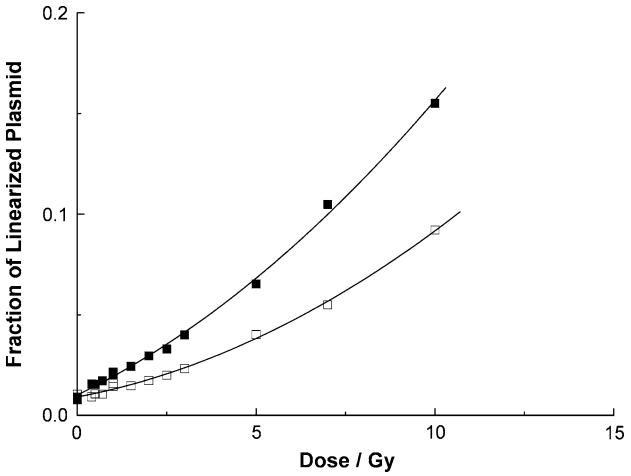

Fig. 4 Formation of linearized plasmid resulting from gamma irradiation with and without subsequent enzyme incubation. Plasmid pHAZE was irradiated and incubated under the same conditions as described for Fig. 3 (same symbols, except *square* instead of *circular*). The fraction of the plasmid in the linearized form was also assayed electrophoretically and plotted against the dose of gamma radiation. Both of the data sets were fitted with a least mean square second-order polynomial of the form $y = ax^2 + bx + c$. From the slopes at zero dose b, the radiation chemical yields of DSB formation under these conditions were (1, neither enzyme) 7.09×10^{-5} μmol J^{-1} and (4, both enzymes) 1.67×10^{-4} μmol J^{-1}

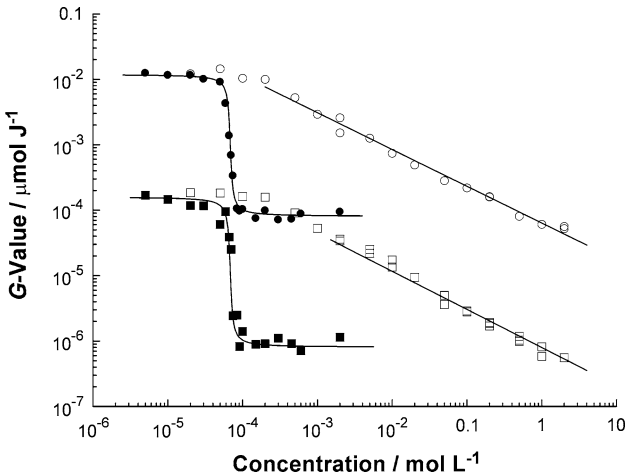

Fig. 5 Effects of glycerol (*open symbols*) or tetra-arginine (R_4, *closed symbols*) on the SSB (*circular symbols*) and the DSB (*square symbols*) yields produced in pHAZE by gamma irradiation with a post-irradiation incubation in the absence of any added enzyme. Strand break yields were measured by constructing yield dose plots similar to those shown in Fig. 3 (for SSBs) and Fig. 4 (for DSBs). The four data sets were fitted approximately with linear or arctan functions simply to assist in distinguishing them, not to imply any description of them with a physical model

various excesses of sodium ions (in the form of its perchlorate salt, which does not affect the radiation chemistry of the solution) were present during irradiation, but the R_4^{4+} concentration was held constant at 1.4×10^{-4} mol l^{-1}. This ligand concentration is more than sufficient to produce the extensive aggregation (Figs. 1, 2) and attenuation in SSB and DSB yields (Fig. 5) described above, in the absence of any added sodium perchlorate.

When sufficient sodium perchlorate was present during irradiation, it was able to prevent this attenuation from taking place. Figure 6 shows that the SSB and DSB yields recovered from their attenuated to their unattenuated values as the total sodium ion concentration (which included the 1.5×10^{-2} mol l^{-1} contribution made by the phosphate buffer system) during irradiation was increased over the range of ca. 3×10^{-2}–5×10^{-2} mol l^{-1}. Further increases in the sodium ion concentration had no additional effect. Note that again this large effect takes place over a characteristically narrow concentration range. In contrast, there was no effect of the additional presence during irradiation of sodium perchlorate on the SSB or DSB yield observed after irradiation in the presence of glycerol (not shown). Thus, in our system, the addition of sodium perchlorate after gamma irradiation has the effect of reversing the aggregation of pHAZE by R_4^{4+} and therefore permitting access to the plasmid by the enzymes FPG and endo III (Newton et al. 2004).

The effect of post-irradiation incubation with FPG and endo III is shown in Fig. 7. The gamma irradiation conditions were 1.4×10^{-4} mol l^{-1} R_4^{4+}, and either zero or 5×10^{-2} mol l^{-1} sodium perchlorate. After irradiation, the sodium perchlorate concentrations were both made equal at 5×10^{-2} mol l^{-1}. With the subsequent incubation in the absence of any added enzymes, the SSB and DSB yields under these conditions were either $G(\text{SSB}) = 7.48 \times 10^{-5}$ μmol J^{-1} and $G(\text{DSB}) = 8.89 \times 10^{-7}$ μmol J^{-1} (zero sodium perchlorate, see Fig. 5) or else $G(\text{SSB}) = 1.04 \times 10^{-2}$ μmol J^{-1} and $G(\text{DSB}) = 7.09 \times 10^{-5}$ μmol J^{-1} (5×10^{-2} mol l^{-1} sodium perchlorate, taken from Figs. 3 and 4). After making the sodium perchlorate concentrations equal, these irradiated samples were also split into aliquots and incubated with several different limiting concentrations of both FPG and endo III. These enzyme concentrations covered a tenfold range and were chosen so that they were significantly lower than those required to convert to strand breaks all of the lesions produced by the gamma irradiation. The purpose was to compare the increase in the DSB yield (for irradiation in the absence or presence of sodium perchlorate) with the increase in the SSB yield (for irradiation in the presence of sodium perchlorate) by incubation under identical conditions.

With no enzyme incubation, the SSB and DSB yields serve as baseline values and are symbolized as $G_0(\text{SSB})$ and $G_0(\text{DSB})$. So for example, the increase in the SSB and DSB yields for the data plotted in Figs. 3 and 4 (this irradiation was in the presence of 5×10^{-2} mol l^{-1} sodium perchlorate) was, respectively, 1.46-fold and 2.36 fold. This may be symbolized as $G(\text{SSB})/G_0(\text{SSB}) = 1.46$ and

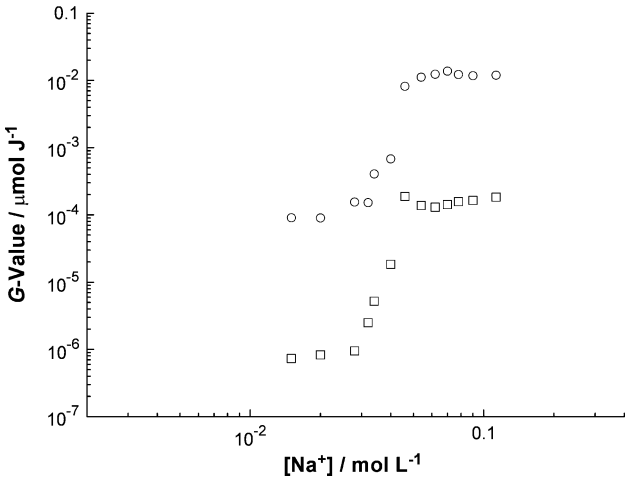

Fig. 6 Effect of the presence during irradiation of sodium perchlorate on the SSB (*circle*) and DSB (*square*) yields produced in plasmid DNA in the presence of 1.4×10^{-4} mol l^{-1} tetra-arginine and a subsequent incubation in the absence of any added enzymes. The total sodium ion concentration plotted on the X-axis includes the contribution made by the phosphate buffer components. Strand break yields were quantified using the method shown in Figs. 3 and 4

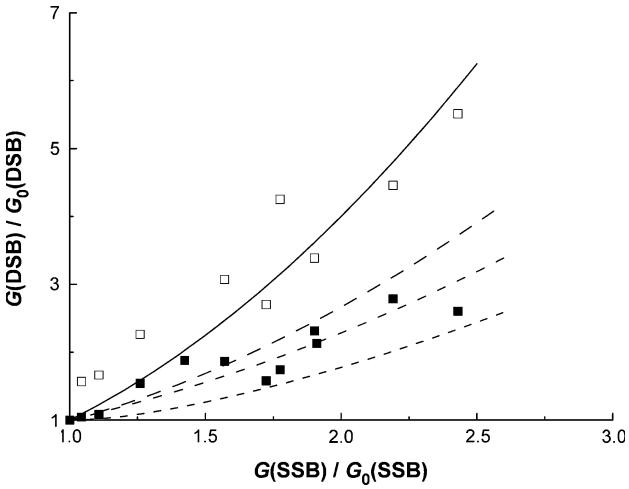

Fig. 7 Effect of the absence or presence of sodium perchlorate during irradiation in the presence of tetra-arginine (1.4×10^{-4} mol l^{-1}) on the increase in the DSB yield produced by a later enzyme incubation. SSB and DSB yields were quantified by constructing yield dose plots such as those depicted in Figs. 1 and 2, respectively. The enzyme-associated increase in the DSB yield after irradiation of the plasmid in the presence of 5×10^{-2} mol l^{-1} sodium perchlorate (*open symbol*) or in its absence (*closed symbol*) plasmid was plotted against the increase in the SSB yield (produced by the same enzyme incubation conditions) after irradiation in the presence of 5×10^{-2} mol l^{-1} sodium perchlorate. The *lines* plotted in this figure represent the theoretical relationships between the increases in SSB and DSB yields which would be expected for four different distributions between the two complementary DNA strands of multiple individual lesions that are substrates for the enzymes FPG and endo III located sufficiently close to each other to result in DSB formation. These are 1:1 (*solid line*), 2:1 (*long dash*), 3:1 (*medium dash*), and 2:2 (*short dash*). Please see the "Discussion" for details

$G(\mathrm{DSB})/G_0(\mathrm{DSB}) = 2.36$ for identical enzyme incubations. Therefore, these two values are plotted against each other (open symbol) in Fig. 7. Increases in DSB yields were also determined after irradiation in the absence of sodium perchlorate. The yields in these cases were of course some two orders of magnitude lower (see Fig. 5), with the value of $G_0(\mathrm{DSB})$ being taken as 8.89×10^{-7} μmol J^{-1} (see above). These $G(\mathrm{DSB})/G_0(\mathrm{DSB})$ values also appear in Fig. 7.

In general, the enzyme-associated increases in the DSB yields were significantly larger after irradiation in the presence of sodium perchlorate (up to fivefold) than after irradiation in its absence (up to only threefold). In addition to the experimental observations, Fig. 7 also contains four lines representing the predicted correlation between the increases in the SSB and DSB yields for four different distributions between the two DNA strands of lesions which are substrates for FPG or endo III and are converted by their activity into SSBs or DSBs (see below).

Discussion

Ligand–plasmid interaction

The results of all five assays shown in Figs. 1 and 2 reveal a large change in the physical properties of the plasmid over a narrow range of ligand concentration extending from about 5×10^{-5} to 7×10^{-5} mol l^{-1}. The light scattering data clearly indicate that above this concentration of the ligand, the plasmid is aggregated into large particles which can be rapidly sedimented. These particles contain essentially all of the plasmid, since once they are pelleted, the remaining solution contains no detectable nucleic acid material as assayed by both UV absorption and ethidium fluorescence.

In the presence of the intercalating fluorescent probe ethidium, the observation of an altered emission spectrum of decreased intensity is suggestive of an alteration in the conformation of the plasmid. Since this change takes place over a narrow concentration range of the ligand (factor of less than 1.5-fold), it is highly unlikely that it represents a simple competition between ethidium and the ligand for binding sites on the plasmid.

The effect of the ligand on the biochemical reactivity of the plasmid was probed by using the enzyme DNAse I. There was a large decrease in two orders of magnitude in the efficiency with which this enzyme was able to catalyze phosphate diester hydrolysis. Again, the narrow concentration range over which this effects occurs argues against a competitive inhibition of the enzyme. The formation of large particles containing all of the plasmid suggests instead that a more likely mechanism is a physical protection in

which the enzyme remains in solution and is unable to gain access to the aggregates.

The ligand concentration at which all of these events approach their asymptotic values is about 7×10^{-5} mol l^{-1}. Assuming that each tetra-arginine ligand carries four positive charges, this corresponds to a cation concentration of $4 \times 7 \times 10^{-5} = 2.8 \times 10^{-4}$ mol l^{-1}. Assuming a mean molecular mass of 330 g mol^{-1} per nucleotide residue, the plasmid concentration of 100 μg ml^{-1} is equivalent to a phosphate anion concentration of $100 \times 10^{-6} \times 10^3/330 = 3.0 \times 10^{-4}$ mol l^{-1}. The close agreement between these oligocation and polyanion concentrations suggests that a very nearly quantitative binding of the ligand to the plasmid produces large changes in physical and chemical properties of the plasmid only when an extensive neutralization of the phosphate groups has taken place.

All of these observations are consistent with the suggestion that the ligand R_4^{4+} acts to condense the plasmid. The electrostatic nature of the interaction between them is consistent with the ionic strength-dependent reversal of the characteristic physical properties of light scattering and sedimentation associated with aggregation (not shown here, although we have reported upon it previously (Newton et al. 2004; Tsoi et al. 2010)). We argue that the high local concentrations present in these aggregated particles offer a promising model system with which to study DNA damage by ionizing radiation under conditions that avoid some of the artifacts associated with previously employed experimental approaches. These include dehydration, freezing, and the use of very high scavenger concentrations.

Radiosensitivity

With glycerol, both the SSB and DSB yields decrease gradually in a manner typical of a competition between it and the plasmid for a reactive intermediate produced by the action of gamma rays on the aqueous medium (Krisch et al. 1991). It is well known that the hydroxyl radical is the species responsible (von Sonntag 2006).

The large changes in physical properties observed over a narrow concentration range of the ligand were very well correlated with its similarly large effects upon the SSB and DSB yields produced in the plasmid by gamma irradiation (compare Fig. 5 with Figs. 1, 2). These breaks were produced by the hydroxyl radical. The conclusion is that the condensation or aggregation of the plasmid into large particles produced an extensive protection against its reactivity with the hydroxyl radical by much the same means as against the reactivity of the enzyme DNAse I. The mechanism appears to be a very limited access to the aggregates by solutes present in the bulk of the solution. Therefore, the local concentrations in these plasmid condensates are very high.

The values of the SSB and DSB yields are comparable with those observed in homogeneous solution in the presence of glycerol only at concentrations in the molar range and less than those observed in irradiated cells. For example, the SSB and DSB yields observed in the presence of the largest glycerol concentrations or with excess (greater than ca. 1×10^{-4} mol l^{-1}) R_4^{4+} were about 1×10^{-4} μmol J^{-1} for SSBs and 1×10^{-6} μmol J^{-1} for DSBs (Fig. 5). Typical values reported for cells are $2–5 \times 10^{-10}$ Gy^{-1} Da^{-1} (equivalent to $2–5 \times 10^{-4}$ μmol J^{-1} under our experimental conditions) for SSBs (Newton et al. 1996) and $3–14 \times 10^{-12}$ Gy^{-1} Da^{-1} (equivalent to $3–14 \times 10^{-6}$ μmol J^{-1}) for DSBs (Newton et al. 1997). The hydroxyl scavenging capacity in these aggregates is presumably similarly large. The result is an extensive decrease in the yield of DNA damage by the indirect effect and also a decrease in the diffusion distance of the hydroxyl radical. A significant contribution by the direct effect can therefore be expected under these conditions, and this model system provides a convenient means with which to study DNA damage by the direct effect.

In the condensed form, the plasmid is unreactive with DNAse I (Fig. 1) and with FPG (Newton et al. 2004). Therefore, it is necessary to reverse the condensation before the damage produced by irradiation in the condensed form, which can be assayed using base excision repair enzymes. Under the experimental conditions we used, this was easily achieved by a modest increase in the ionic strength. A sodium perchlorate concentration of 5×10^{-2} mol l^{-1} is entirely compatible with the ionic requirements of FPG and endo III. Because the plasmid, ligand, and sodium perchlorate concentrations were all identical during the enzyme incubation step, any differential effects of those enzymes are necessarily attributable to the conditions during irradiation.

Enzyme incubation

The action of both FPG and endo III is to convert modified bases to strand breaks by way of an intermediate abasic site. The major base damage product resulting from gamma irradiation which is recognized by FPG is 8-oxoguanine, while pyrimidine glycol species are the major substrates for endo III (Cadet et al. 2000). The experimental observation is of an increase in the SSB and DSB yields over those produced by irradiation alone. Depending to some extent upon the irradiation conditions, an excess of FPG or of endo III typically produces an increase in the SSB yield of ca. twofold, which is consistent with the chromatographically determined yields of their substrates in irradiated DNA targets (Cadet et al. 2000). Since their substrate

specificities are largely (although not entirely) non-overlapping (Harrison et al. 1998), these effects tend to be nearly additive. Incubation with excess base excision repair endonucleases such as FPG and endo III provides a sensitive assay for the product distribution produced in DNA under different conditions or by different types of ionizing radiation. Examples include irradiated cells (Sutherland et al. 2003), particulate radiation (Yokoya et al. 2009); Terato et al. 2008), and soft X-rays (Yokoya et al. 2009).

It is also possible to make use of the increases in SSB and DSB yields produced by incubation with these enzymes to examine the spatial distribution or clustering of DNA damage produced by ionizing radiation (Sutherland et al. 2000). We have argued that by using limiting concentrations of these enzymes and by quantifying the increases in the SSB and DSB yields which result, it is possible to characterize the spatial distribution of damaged bases which are substrates for them (Milligan et al. 2000). Briefly, a smaller increase in the DSB yield produced by enzyme incubation is expected if SSB and base lesions are clustered together. This is because strand break events produced by the enzymes are not detectable if they are produced in close proximity to existing breaks. The magnitude of this effect can be predicted using a simple combinatorial model (Milligan et al. 2001). A separate mechanism may also produce this same effect, because in certain cases the activity of some enzymes may be inhibited by the presence of nearby damages (Chaudhry and Weinfeld 1995).

It is possible to derive an expression for the relative increase in the DSB yield produced by enzyme incubation. This is the ratio $G(\mathrm{DSB})/G_0(\mathrm{DSB})$ which is plotted in Fig. 7. A base damage which is a substrate for FPG and/or endo III is described as an enzyme-sensitive lesion (ESL). Consider a DSB event produced by two hydroxyl radical attacks or direct energy deposition events, one in each of the two complementary strands. Such an event may be represented by the symbol "1:1". With an enzyme incubation, there are three possibilities to consider. These are as follows: (1) both events produce SSBs; (2) one event produces an SSB and the other an ESL; and (3) both events produce ESLs. The second possibility occurs with twice the probability of the other two, so its contribution must be doubled. The DSB yield in the absence of any enzyme incubation is $G_0(\mathrm{DSB})$. The DSB yield observed after enzyme incubation ($G(\mathrm{DSB})$) will be larger because of the contributions made by the ESLs. Because the enzymes are intentionally present in limiting amounts, not all of the ESLs will be converted into SSBs. Only a fraction F of them will be (where $F = 0$ in the absence of any added enzymes). Then for the three possibilities listed above, the yield of DSB events after enzyme incubation is equal to $G(\mathrm{DSB}) = G_0(\mathrm{DSB}) + 2 \times F \times G_0(\mathrm{DSB}) + F^2 \times G_0(\mathrm{DSB})$, respectively. Rearranging this expression for the ratio $G(\mathrm{DSB})/G_0(\mathrm{DSB})$ which is plotted in Fig. 7 yields $G(\mathrm{DSB})/G_0(\mathrm{DSB}) = F^2 + 2F + 1$. Plotting (for many different values of F, which is equivalent to many different although always limiting concentrations of FPG and endo III) this against the ratio $G(\mathrm{SSB})/G_0(\mathrm{SSB})$, which is simply equal to $F + 1$, produces the uppermost curve (solid line) in Fig. 7.

Following a similar argument (Milligan et al. 2001), it is possible to derive a similar expression for a DSB involving three events, two on one strand and one on the other, symbolized by "2:1". This expression is $G(\mathrm{DSB})/G_0(\mathrm{DSB}) = (F + 1)^3/(2F + 1)$. The expressions for "3:1" and "2:2" events are, respectively, $(F + 1)^4/(3F^2 + 3F + 1)$ and $(F + 1)^4/(4F^2 + 4F + 1)$. These are also plotted in Fig. 7. The conclusion to be drawn from these equations is that as the complexity or the clustering of the DNA damage increases, the increase in the DSB yield produced by enzyme incubation is expected to become less pronounced. These theoretical lines can be used to interpret the experimental observations plotted in Fig. 7 if the activities of FPG and endo III are unaffected by nearby lesions, but as we have discussed above this may not be the case. However, both effects of increased clustering drive the observed value of $G(\mathrm{DSB})/G_0(\mathrm{DSB})$ in the same direction. Therefore, we argue that the observation of significantly and consistently smaller values of $G(\mathrm{DSB})/G_0(\mathrm{DSB})$ for plasmid DNA gamma-irradiated in an aggregated form than in homogeneous solution provides evidence in favor of damage clustering in the former target. We suggest that this reflects the nature of the DNA damage produced under conditions where hydroxyl radical diffusion distance is severely limited and/or a significant contribution appears to be from the direct effect.

Acknowledgments This study was supported by PHS grant CA46295.

References

Bloomfield VA (1996) DNA condensation. Curr Opin Struct Biol 6:334–341

Cadet J, Bourdat A-G, D'Ham C, Duarte V, Gasparutto D, Romieu A, Ravanat J-L (2000) Oxidative base damage to DNA: specificity of base excision repair enzymes. Mutat Res 462:121–128

Chaudhry MA, Weinfeld M (1995) The action of Escherichia coli endonuclease III on multiply damaged sites in DNA. J Mol Biol 249:914–922

Chiu S, Oleinick NL (1998) Radioprotection of cellular chromatin by the polyamines spermine and putrescine: preferential action against formation of DNA-protein crosslinks. Radiat Res 149:543–549

Daban J-R (2003) High concentration of DNA in condensed chromatin. Biochem Cell Biol 81:91–99

Goodhead DT (1994) Initial events in the cellular effects of ionizing radiations: clustered damage in DNA. Int J Radiat Biol 65:7–17

Harrison L, Hatahet Z, Purmal AA, Wallace SS (1998) Multiply damaged sites in DNA: interactions with *Escherichia coli* endonucleases III and VIII. Nucleic Acids Res 26:932–941

Krisch RE, Flick MB, Trumbore CN (1991) Radiation chemical mechanisms of single and double-strand break formation in irradiated SV40 DNA. Radiat Res 126:251–259

Lutze LH, Winegar RA (1990) pHAZE: a shuttle vector system for the detection and analysis of ionizing radiation-induced mutations. Mutat Res 245:305–310

Milligan JR, Aguilera JA, Ward JF (1993) Variation of single-strand break yield with scavenger concentration for plasmid DNA irradiated in aqueous solution. Radiat Res 133:151–157

Milligan JR, Aguilera JA, Nguyen TT, Paglinawan RA, Ward JF (2000) DNA strand-break yields after post-irradiation incubation with base excision repair endonucleases implicate hydroxyl radical pairs in double-strand break formation. Int J Radiat Biol 76:1475–1483

Milligan JR, Aguilera JA, Paglinawan RA, Ward JF, Limoli CL (2001) DNA strand break yields after post-high LET irradiation incubation with endonuclease-III and evidence for hydroxyl radical clustering. Int J Radiat Biol 77:155–164

Milligan JR, Aguilera JA, Ly A, Tran NQ, Hoang O, Ward JF (2003) Repair of oxidative DNA damage by amino acids. Nucleic Acids Res 31:6258–6263

Newton GL, Aguilera JA, Ward JF, Fahey RC (1996) Polyamine-induced compaction and aggregation of DNA: a major factor in radioprotection of chromatin under physiological conditions. Radiat Res 145:776–780

Newton GL, Aguilera JA, Ward JF, Fahey RC (1997) Effect of polyamine-induced compaction and aggregation of DNA on the formation of radiation-induced strand breaks: quantitative models for cellular radiation. Radiat Res 148:272–284

Newton GL, Ly A, Tran NQ, Ward JF, Milligan J (2004) Radioprotection of plasmid DNA by oligolysines. Int J Radiat Biol 80: 643–651

Nikjoo H, Goorley T, Fulford J, Takakura K, Ito T (2002) Quantitative analysis of the energetic of DNA damage. Radiat Prot Dosimetr 99:91–98

Padmanabhan S, Zhang W, Capp MW, Anderson CF, Record MT Jr (1997) Binding of cationic (+4) alanine- and glycine-containing oligopeptides to double-stranded DNA: thermodynamic analysis of effects of coulombic interactions and alpha-helix induction. Biochemistry 36:5193–5206

Pogozelski WK, Tullius TD (1998) Oxidative strand scission of nucleic acids: routes initiated by hydrogen abstraction from the sugar moiety. Chem Rev 98:1089–1108

Spinks JWT, Woods RJ (1990) An introduction to radiation chemistry. Wiley, New York

Spotheim-Maurizot M, Ruiz S, Sabattier R, Charlier M (1005) Radioprotection of DNA by polyamines. Int J Radiat Biol 68:571–577

Sutherland BM, Bennett PV, Sidorkina O, Laval J (2000) Clustered damages and total lesions induced in DNA by ionizing radiation: oxidized bases and strand breaks. Biochemistry 39:8026–8031

Sutherland BM, Georgakilas AG, Bennett PV, Laval J, Sutherland JC (2003) Quantifying clustered DNA damage induction and repair by gel electrophoresis, electronic imaging and number average length analysis. Mutat Res 531:93–107

Terato H, Tanaka R, Nakaarai Y, Nohara T, Doi Y, Iwai S, Hirayama R, Furusawa Y, Ide H (2008) Quantitative analysis of isolated and clustered DNA damage induced by gamma rays, carbon ion beams, and iron ion beams. J Radiat Res (Tokyo) 49:133–146

Tsoi M, Do TT, Tang V, Aguilera JA, Perry CC, Milligan JR (2010) Characterization of condensed plasmid DNA models for studying the direct effect of ionizing radiation. Biophys Chem 147:104–110

Vilfan ID, Conwell CC, Sarkar T, Hud NV (2006) Time study of DNA condensate morphology: implications regarding the nucleation, growth, and equilibrium populations of toroids and rods. Biochemistry 45:8174–8183

von Sonntag C (2006) Free radical induced DNA damage and its repair: a chemical perspective. Springer, New York

Ward JF (1994) The complexity of DNA damage-relevance to biological consequences. Int J Radiat Biol 71:347–363

Warters RL, Newton GL, Olive PL, Fahey RC (1999) Radioprotection of human cell nuclear DNA by polyamines: radiosensitivity of chromatin is influenced by tightly bound spermine. Radiat Res 151:354–362

Yokoya A, Cunniffe SM, Watanabe R, Kobayashi K, O'Neill P (2009) Induction of DNA strand breaks, base lesions and clustered damage sites in hydrated plasmid DNA films by ultrasoft X rays around the phosphorus K edge. Radiat Res 172:296–305